CHARACTERISATION OF SUBCHONDRAL BONE REPAIR FOLLOWING TRANSPLANTATION OF BIOREACTOR-MANUFACTURED AUTOLOGOUS OSTEOCHONDRAL GRAFT IN A SHEEP MODEL

P. Kostešić[1,§], A. Vukasović Barišić[2,§], I. Erjavec[3], M. Pušić[4], D. Hudetz[5,6], D. Matičić[1], D. Vnuk[1], M. Vučković[1] and A. Ivković[5,7,8,9,*]

[1] Department of Surgery, Ophthalmology and Orthopaedics, Faculty of Veterinary Medicine, University of Zagreb, Zagreb, Croatia
[2] General Hospital Bjelovar, Bjelovar, Croatia
[3] Laboratory for Mineralised Tissue, School of Medicine, University of Zagreb, Zagreb, Croatia
[4] Division of Molecular Biology, Faculty of Science, University of Zagreb, Zagreb, Croatia
[5] Department of Orthopaedic Surgery, University Hospital "Sveti Duh", Zagreb, Croatia
[6] St. Catherine's Hospital, Zabok, Croatia
[7] School of Medicine, University of Zagreb, Zagreb, Croatia
[8] Department of Biotechnology, University of Rijeka, Rijeka, Croatia
[9] University of Applied Health Sciences, Zagreb, Croatia
[§] These authors contributed equally to this work

Abstract

To date, no single approach to the treatment of osteochondral defects has resulted in satisfactory long-term outcomes, especially in a young and active human population. Emerging innovative tissue engineering strategies, including the use of composite scaffolds, novel cell sources and bioreactors, have shown promising results. However, these techniques need to be validated in translational animal models before they can be implemented in clinical practice. The aim of the present study was to analyse morphological and microarchitectural parameters during subchondral bone repair following transplantation of bioreactor-manufactured autologous osteochondral grafts in a sheep model. Animals were divided into 4 treatment groups: nasal chondrocyte (NC) autologous osteochondral grafts, articular chondrocyte (AC) autologous osteochondral grafts, cell-free scaffolds (CFS) and empty defects (EDs). After 6 weeks, 3 months and 12 months, bone remodelling was assessed by histology and micro-computed tomography (μCT). Although gradual remodelling and subchondral bone repair were seen in all groups across the time points, the best results were observed in the NC group. This was evidenced by the extent of new tissue formation and its best integration into the surrounding tissue in the NC group at all time points. This also suggested that nasal septum chondrocyte-seeded grafts adapted well to the biomechanical conditions of the loaded joint surface.

Keywords: Subchondral bone, osteochondral graft, tissue engineering, computerised tomography, bioreactors, cartilage repair, animal model.

***Address for correspondence**: Alan Ivković, MD, PhD, Department of Orthopaedic Surgery, University Hospital "Sveti Duh", Sveti Duh 64, 10000 Zagreb, Croatia.
Telephone number: +385 912445539 email: alan.ivkovic@gmail.com

Copyright policy: This article is distributed in accordance with Creative Commons Attribution Licence (http://creativecommons.org/licenses/by/4.0/).

List of Abbreviations

AC	articular chondrocytes
BS	bone surface
BV/TV	bone volume/tissue volume
CFS	cell-free scaffold
Co.Th	cortical thickness
Conn.d	connectivity density
DMEM	Dulbecco's modified Eagle medium
ED	empty defect
EDTA	ethylenediaminetetraacetic acid
GMP	good manufacturing practice
GPU	graphics processing unit
HE	haematoxylin-eosin
HEPES	N-2-hydroxyethylpiperazine-N'-2-ethanesulfonic acid

ICRS	International Cartilage Repair Society
NC	nasal chondrocyte
Mg-HA	magnesium-doped hydroxyapatite
OA	osteoarthritis
PFA	paraformaldehyde
ROI	region of interest
SD	standard deviation
SMI	structure model index
Tb.N	trabecular number
Tb.Sp	trabecular separation
Tb.Th	trabecular thickness
μCT	micro-computed tomography

Introduction

The osteochondral unit is the fundamental architectural building block of diarthroidal joints. It consists of articular cartilage, calcified cartilage and subchondral cortical and trabecular bone (Duncan *et al.*, 1987). Historically, subchondral bone has been overlooked in the management of OA and cartilage defects and the focus of research and treatment has almost exclusively been on the chondral component of the osteochondral unit. Recently, subchondral bone repair has at long last come under the spotlight of joint disease and OA research and management, and it is well established that the osteochondral unit must be fully restored/maintained for any meaningful cartilage repair to occur (Gomoll *et al.*, 2010).

The subchondral bone consists of two integrated, yet different structural elements: subchondral bone plate and trabecular subchondral bone. The subchondral bone plate is a thin cortical lamella, bound to the calcified layer of the articular cartilage, and ultimately supported by the trabecular bone underneath (Hunziker *et al.*, 2002; Milz and Putz, 1994). The subchondral bone plate merges into a network of trabecular bone, forming a more porous and metabolically active subchondral trabecular bone (Goldring and Goldring, 2016). Subchondral trabecular bone provides mechanical and nutritional support to the articular cartilage and undergoes constant adaptation to the biomechanical changes in its surroundings (Madry *et al.*, 2010). It is the primary structure of transarticular load bearing and allows for normal joint articulation and movement. Untreated chondral, osteochondral and subchondral lesions can lead to irreversible damage and degeneration of the osteochondral unit and cause OA.

Alterations to the subchondral bone following OA and cartilage trauma are not merely secondary manifestations but also active components of the disease, contributing to its severity. In addition to OA, a variety of articular cartilage repair procedures (*e.g.* bone marrow stimulation techniques) induce pathological remodelling of subchondral bone, directly influencing clinical outcomes as well as potential revision procedures (Saris *et al.*, 2009). Changes to the subchondral bone include (1) upward migration of the subchondral bone plate, (2) formation of intralesional osteophytes, (3) subchondral cyst appearance and (4) impairment of the osseus microstructure (Orth *et al.*, 2013). These alterations have been observed in both humans and animals (Fisher *et al.*, 2014; Lajeunesse *et al.*, 1999; Mithoefer *et al.*, 2005; Orth *et al.*, 2013; Pepe *et al.*, 2010; Siu *et al.*, 2004). Since its advent, μCT has been an invaluable tool for bone microarchitecture analysis (Feldkamp *et al.*, 1989). As the microarchitecture of the subchondral bone is three-dimensional and complex, a combination of different parameters is used to interpret the remodelling processes.

To date, no single approach to the treatment of osteochondral defects has resulted in satisfactory long-term outcomes, especially in a young and active human population. Techniques focusing on mechanical or biological osteochondral repair have been developed, providing a framework for a holistic approach, but each with its own limitations. These techniques include osteotomies, arthroplasty, microfractures, abrasion arthroscopy, autologous osteochondral transplantation (mosaicplasty) and autologous chondrocyte transplantation (Nikolaou and Giannoudis, 2017). Advances in cell-seeded multiphasic tissue scaffolds and matrices (Dorotka *et al.*, 2005; Jeon *et al.*, 2014; Kon *et al.*, 2010; Schleicher *et al.*, 2012; Tampieri *et al*, 2008), bioreactor-derived tissue cultures (Tonnarelli *et al.*, 2016; Wendt *et al.*, 2005) and mesenchymal cell re-differentiation (Calabrese *et al.*, 2016; Lee *et al.*, 2014; Malda *et al.*, 2004) offer a combined, highly technological and potentially viable option for the treatment of osteochondral defects. NCs have been investigated as a potential cell source for articular defect treatment, an alternative to ACs, currently in clinical use (Mumme *et al.*, 2016a; 2016b).

The aim of a previously published study by Vukasovic *et al.* (2019) was to establish an automated manufacturing platform for the production of NC-based engineered grafts and to assess such grafts in a clinically relevant animal model. Published data focused on the histological assessment of articular cartilage. The aim of the present study was to analyse the subchondral bone and its microarchitecture during repair.

Material and Methods

Study design

A large-animal study was performed at the Faculty of Veterinary Medicine (University of Zagreb, Zagreb, Croatia) with approval from the local ethics committee (University of Zagreb, Faculty of Veterinary Medicine, Class 640-01/12-17/99, Reg. No. 251-61-01/139-12-2) and the national authorities (Ministry of Agriculture of Croatia; Class UP/I-322-01/13-01/79, Reg. No. 525-10/0255-13-3). 24 skeletally mature female German Wustenrot sheep,

1-3 years old (57.2 ± 13.7 kg) were included in the study. The animals were randomly assigned to 4 groups (described further in the manuscript), each group consisting of 6 sheep.

The protocol used included two surgical procedures on a right stifle joint of each animal. The aim of the first surgical procedure was to create chondral defects and harvest cartilage for chondrocyte culturing and graft production. After the first procedure, a 6-week period enabled graft production as well as chronification to take place within the defect site. This approach was chosen to create a challenging, clinically relevant model. During the second surgical procedure, chronified chondral defects on femoral condyles of the right knee were converted to ostechondral defects and bioreactor-manufactured grafts were implanted (Fig. 1). In the NC group, autologous osteochondral grafts (scaffold + NCs) were implanted in the osteochondral defects. AC group had autologous osteochondral grafts (scaffold + ACs) implanted in the osteochondral defects. Osteochondral defects in the CFS group were treated with CFSs while the group ED served as negative control in which osteochondral defects were left untreated (sham surgery).

Animal admission

The sheep were delivered to the Faculty of Veterinary Medicine at least 24 h prior to the procedure to acclimatise and accommodate themselves to the new surroundings. Food was withheld for at least 24 h and water for 8-12 h prior to the surgery, depending on the environmental temperatures and the condition of each animal. For identification, each animal received an ear tag and microchips were placed under the skin at the back of the neck between the shoulder blades on the dorsal midline.

Anaesthesia and pain management

All animal procedures were performed under general inhalation anaesthesia, using an open medial parapatellar approach (Vukasovic *et al.*, 2019).

Intraoperative analgesia was maintained at a constant perfusion rate of 0.2 µg/kg/min fentanyl intravenously (Fentanyl injections, Janssen Pharmaceutica NV). Post-operative analgesia was provided using meloxicam (Movalis, Boehringer Ingelheim) in an initial intramuscular dose of 0.2 mg/kg followed by an intramuscular dose 0.1 mg/kg once a day, for a minimum of 3 d.

Surgical procedure for defect creation and biopsy harvesting

First surgical procedure - defect creation and articular cartilage harvesting

A medial parapatellar approach to the right knee was used for chondral defect creation and articular cartilage harvesting. A full-thickness cartilage defect, 4 mm in diameter, was made in the weight-bearing area of medial and lateral femoral condyles, using a cylindrical biopsy punch to mark the circumference of the defect, which was then cut out using a scalpel and a small curette. The cartilage biopsy (2 chondral discs measuring 4 mm in diameter each) were used for AC graft production. The whole chondral layer was removed, taking special care not to damage the subchondral bone. Two defects were created in the right knee of each animal and the joints were flushed with saline. Next, the joint capsule and medial fascia of the stifle joint were closed in one layer with interrupted sutures using a monofilament absorbable suture. Subcutis and skin were closed routinely. The obtained articular cartilage was washed with saline, dried and stored in complete medium [92 % DMEM, 5 % fetal bovine serum, 1 % penicillin-streptomycin-glutamine, 1 % HEPES, 1 % sodium pyruvate] at 4 °C for transport to the GMP facility where the AC grafts would be produced from this tissue.

NC biopsy

In the NC group, nasal cartilage was harvested from the nasal septum. A vertical incision was made in the rostral nasal mucous epithelium. Tunnels were prepared vertically along the nasal septum and a blunt periosteal elevator was advanced caudally to elevate the mucosa from the nasal cartilage. An 8 mm cylindrical skin biopsy punch was used to harvest a full-thickness nasal septum cartilage graft. Then, the biopsy was cleaned of any residual perichondrium, flushed with saline, blotted with sterile gauze and

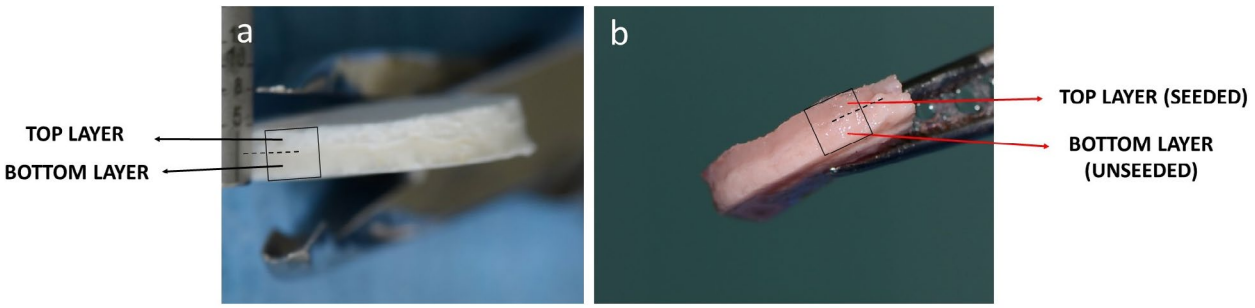

Fig. 1. Bi-layered biomimetic osteochondral scaffold. (**a**) A 3 mm thick top layer consisting of equine type I collagen and the 2 mm thick bottom layer made of a mineralised blend of type I collagen and Mg-HA. (**b**) The construct engineered in the bioreactor. The upper (cartilage) layer was seeded with articular or nasal septum chondrocytes, the bottom layer was acellular (and responsible for the integration into surrounding subchondral bone).

stored in complete medium at 4 °C for transport to the GMP facility for the NC graft production.

For the NC graft production, the mucosa was sutured in one layer using absorbable multifilament suture material.

Animal aftercare

Following surgery, sheep were kept in the clinic for 5 d. Surgical wounds were covered with sterile bandages. The operated limbs were not immobilised in any way. The animals were kept in small pens to reduce ambulation. After 5 d at the clinic, they were transported back to the family farm where the sheep were held under natural conditions with no ambulation restrictions. They were checked daily by a veterinary surgeon and weekly by researchers.

Bioreactor-based graft production

Harvested nasal and articular cartilage samples were transported to the GMP facility to produce cartilage grafts. Grafts were manufactured in automated perfusion bioreactor system, as previously described by Vukasovic *et al*. (2019). Briefly, the cartilage biopsy was enzymatically digested using a digestion bioreactor (Octane, Kingstone, Canada), which automatically delivered the necessary solutions in a tightly controlled manner. Then, the freshly isolated chondrocytes were introduced in the T-CUP perfusion bioreactor (Cellec Biotek AG, Basel, Switzerland) where they were uniformly seeded, expanded and differentiated directly within a porous 3D bilayered scaffold (Finceramica, Faenza, Italy) The bilayered biomimetic osteochondral scaffold measured 25 mm in diameter and 5 mm in thickness. It consisted of a 3 mm thick upper layer made of equine type I collagen and a 2 mm thick bottom layer made of a mineralised blend of type I collagen and Mg-HA, mimicking the structure and biochemistry of cartilage and subchondral bone, respectively. Chondrocytes were seeded into the scaffold under alternating perfusion flow at a perfusion rate of 1 mm/s for 16 h in complete medium. Following seeding phase, grafts were perfused for 3 weeks at a perfusion rate of 100 μm/s in proliferating medium. After the proliferation phase, culture medium was replaced with differentiating medium and grafts were cultured in the bioreactor for the following 2 weeks. After 5 weeks of culture in the perfusion bioreactor, viable cartilaginous grafts (Fig. 1) were transported to the veterinary clinic for the implantation surgery.

Second surgical procedure - graft implantation procedure

The procedures for the second surgical exposure of the right stifle joint were the same as described for the first step surgery. First, previously inflicted cartilage defects were visualised. At this point cartilage defects were uneven, with fissures that extended to the cartilage surface surrounding the

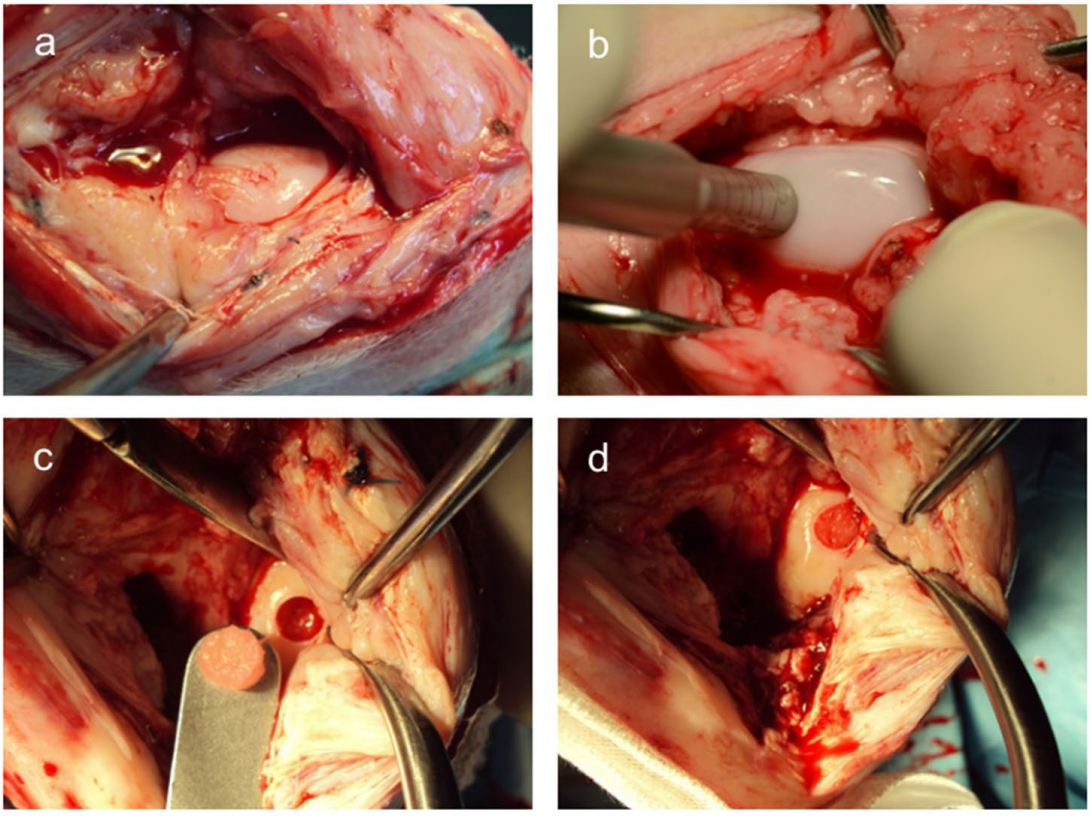

Fig. 2. The second surgery with defect conversion and construct implantation. (**a**) Chronic full-thickness chondral 4 mm defect on the weight-bearing surface of the medial femoral condyle. (**b**) Conversion of the chronic full-thickness chondral defect into 6 × 5 mm osteochondral defect using a mosaic-plasty kit. (**c**) A size-matched construct prepared for implantation into the osteochondral defect. (**d**) An implanted graft, press-fitted into the defect, flushed with the articular surface.

defect. Mild oedema and hyperaemia of the synovial membrane were also present. These chronified cartilage defects were converted to 6 mm diameter × 5 mm deep osteochondral defects (Fig. 2). Only half of the bioreactor-produced AC and NC grafts (25 mm diameter, 5 mm hight) were used for implantation. The other half was used for histological and biochemical analysis, which was beyond the scope of the present study. A 6 mm cylindrical biopsy punch was used to cut two implants from each AC and NC graft. These were press-fitted into the defect site on the medial and lateral condyle, flushed with the surrounding joint surface. In the CFS group, the defect sites were treated with CFSs. ED sheep underwent a defect conversion without implantation. 30 ranges of motion cycles were performed to check the implant's stability. The joints were flushed and closed in the same way as in the first surgery.

Postoperative analgesia and care were the same as for defect creation procedures. Surgical wounds were covered using sterile bandages and the operated limbs were not immobilised in any way. The animals were kept for 5 d at the clinic in small pens to reduce ambulation, then they were transferred to the family farm where the sheep were held under natural conditions with no ambulation restrictions until the end of the study.

Euthanasia time points and explant procedure

At the end of the study, the animals were pharmacologically euthanised. 2 animals from each group were euthanised after 6 weeks, 3 months and 12 months. After euthanasia, the joint was exposed and visualised and the osteochondral blocks were explanted. The osteochondral block containing defect site and surrounding healthy osteochondral tissue of the femoral medial and lateral condyle were removed and cut in half using a cooled oscillating bone saw (n = 4 defects per each group, except NC 12 months where there was n = 2 defects) (Fig. 3**a**,**b**). This produced osteochondral blocks measuring about 10 × 10 × 5 mm. The blocks were fixed in 4 % PFA for at least 48 h. Then, they were scanned using a μCT device, after which they were decalcified in 15 % EDTA, dehydrated and embedded in paraffin wax. For histological examination, specimens were stained with HE, safranin O and picrosirius red (3 slides for each staining). Two blinded and independent observers, experienced in histology, examined the slides using a bright-field and polarised-light microscope and evaluated them following the ICRS II histology score (Mainil-Varlet *et al.*, 2010). One joint score was given for each parameter after examining all 9 slides (Vukasovic *et al.*, 2019).

μCT analysis

Collected osteochondral blocks were scanned using a Skyscan 1076 μCT device (Bruker). The blocks were prepared by tightly wrapping them in a plastic foil to prevent drying during the scan. Scanning was done at 20 kV and 200 μA, yielding an isotropic resolution of 18 μm. To prevent beam hardening, a 0.5 mm thick aluminium filter was used. The rotational step was 0.5° throughout 198° with a frame averaging set at 2. Obtained images were reconstructed using the NRecon software (Bruker) by employing GPU-based reconstruction. Sample analysis was done using the CTAn software (Bruker). Two ROIs were manually delineated: subchondral plate (further in text: plate) and subchondral trabecular bone (further in text: trabecular bone) (Fig. 3**c**). For all samples, the sizes of the ROIs (height × width) were the same. Plate ROI encompassed just the condyle cortical bone with a size of 1.4 × 7 mm. Trabecular bone ROI that spanned beneath the plate ROI, with a size of 5 × 7 mm, ensured the inclusion of the whole defect. Parameters that were measured included BV/TV, BS, Co.Th for the plate and trabecular parameters such as Tb.Th, Tb.N, Tb.Sp and Conn.d.

Statistical analysis

Quantitative histology data are presented as mean ± SD. Quantitative μCT data are presented as median with interquartile range, along with mean ± SD. To analyse differences, the Kruskal-Wallis test was used. *Post-hoc* inter-group differences were calculated by the Mann-Whitney test. $p < 0.05$ was considered statistically significant. All analyses were performed

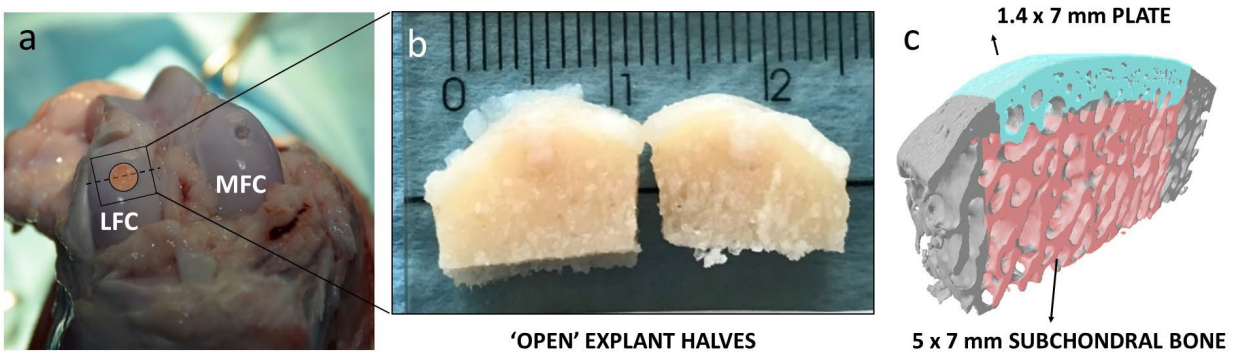

Fig. 3. A view of the distal femur with the defect sites and explanted blocks. (**a**) A representative axial view of the right knee with defects on the lateral (LFC) and medial (MFC) femoral condyle. (**b**) Explanted defect with surrounding tissue cut into two halves selected ROI. (**c**) Plate and subchondral bone are shown in a reconstructed μCT image of the explanted block.

using the IBM SPSS Statistics software (version 22.0. Armonk, IBM Corp).

Results

All 24 animals underwent successful procedures, without complications. After the surgical procedures, they recovered well and were allowed weight bearing within a few hours. No animals showed signs of superficial or deep surgical-site infection. The animals spent the appropriate time until implantation or euthanasia at the farm, without restriction in their movement. Unfortunately, one animal from the NC group-12 months was lost for reasons unrelated to the study (fasciolosis), at a stage of the study when it was impossible to replace it due to the expiration of the study permit.

The grafts were implanted by press-fit fixation and all stayed in the defect until the end of the study. Also, there was no detachment of the graft or scaffold from the defect or delamination of cartilage from the bone.

Histology

Histological evaluation at 6 weeks

At 6 weeks, defect sites were distinguishable in all specimens (Fig. 4, top row). Incomplete defect filling with obvious central cavities (doughnut effect) was observed in all groups. Repaired tissue in the defects varied from granulation to loose connective tissue. Adjacent cartilage could be seen protruding towards the defect. Areas of hyaline cartilage were found at the bottom and on the sides of the defect, adjacent to subchondral bone. Hyaline cartilage islands were present in the upper regions of the NC defects (Fig. 5). The repair tissue was integrated with adjacent cartilage and bone, without cracks or fissures. At this point, there was no significant subchondral bone restoration, only marginal ossification was present. ICRS II score indicated the best repair in the NC group, especially in terms of surface architecture, which was significantly smoother in the NC compared to AC ($p = 0.043$), CFS ($p = 0.043$) and ED ($p = 0.02$) groups. Abundant vascular spaces were observed within the scaffold pores, especially in the CFS group (Fig. 6). Leukocytes, macrophages and giant cells were also present. Inflammation was significant in the AC compared to CFS and ED groups ($p = 0.02$ for both comparisons) (Fig. 7**a**,8).

Histological evaluation at 3 months

At 3 months, defects were still clearly distinguishable. The defects were better filled with newly formed tissue (*i.e.* larger volume of tissue occupied the defect) compared to 6 weeks, notably in the ED and NC groups (Fig. 9). Hyaline cartilage dominated the upper layer of the NC group and it extended deeper into the defect (Fig. 4 middle row,6). Subchondral bone restoration with active ossification was evident across all groups, the most extensive in the NC group. ED defects were filled by mostly loose connective tissue, with areas of both intramembranous and endochondral ossification in the periphery of the defects (Fig. 10). At 3 months, a subchondral cyst was observed in the ED group. The restoration of osteochondral tissue in the AC group was poor, with defects filled with loose connective tissue and occasional marginal ossification. CFS defects presented mostly fibrotic tissue, with marginal ossification and cartilage restoration with central cavities. Some residual scaffold material was still present in the CFS, AC and NC groups. Macrophages and leukocytes were scarce in the NC group and prevalent in the AC and CFS groups. Giant cells were also observed in AC and CFS groups.

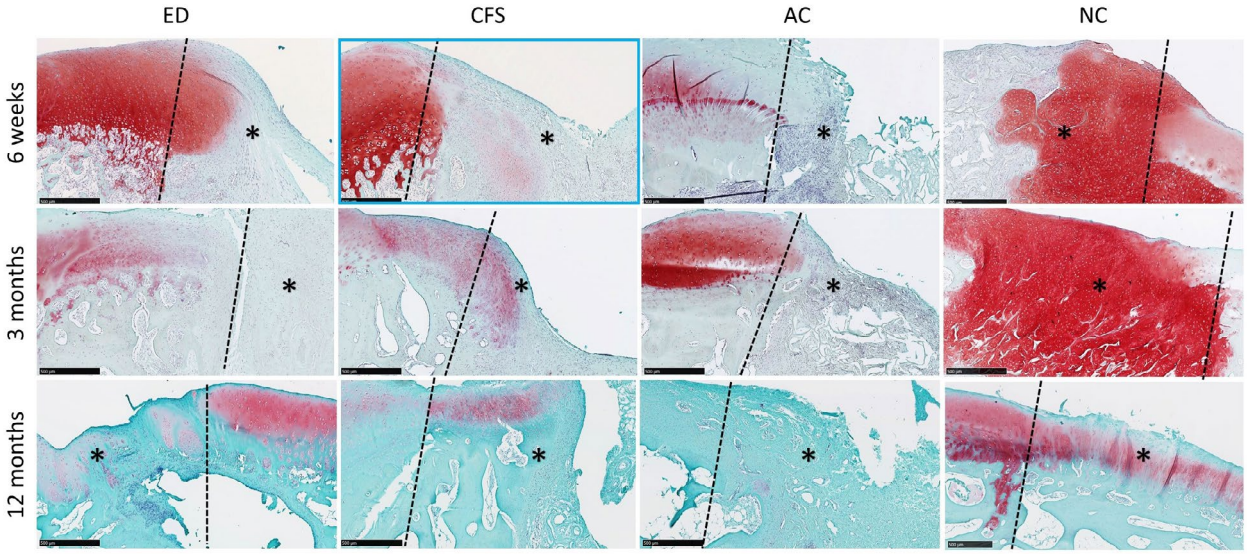

Fig. 4. Explants from all 3 time points stained with safranin O. Dashed line indicates border between defect and surrounding native osteochondral tissue. Asterisk marks the defect tissue in every sample. Scale bar: 500 μm. The highest score for matrix staining and tissue morphology was in the NC group. The 6 week CFS sample in the blue frame is depicted again in Fig. 6.

ICRS II histological scores were significantly higher for NC-treated defects compared to AC- and CFS-treated defects for the parameters tissue morphology ($p = 0.02$ for both comparisons), matrix staining ($p = 0.02$), cell clustering ($p = 0.028$ for AC; $p = 0.02$ for ED), surface architecture ($p = 0.02$) and deep zone morphology ($p = 0.02$). NC had also significantly higher scores than CFS for cell clustering and surface architecture ($p = 0.02$). ICRS II score for vascularisation ($p = 0.02$ for both comparisons) and overall score was significantly higher in both NC and ED groups compared to AC ($p = 0.02$ and $p = 0.043$, respectively) (Fig. 7**b**).

Histological evaluation at 12 months

At 12 months, the healing improved in all groups. Defect sizes had overall decreased and a more complete osteochondral restoration was achieved (Fig. 11). There was no appreciable demarcation line between implants and surrounding tissue, especially in the subchondral bone. Repair of chondral layer varied, from fibrous tissue to hyaline cartilage. Fibrous tissue was observed in the chondral region of AC and CFS defects, with hyaline cartilage located only marginally. In the ED group, the bone was covered with a feeble layer of fissured, discontinuous cartilage or fibrous tissue and was not levelled with the surrounding articular surface. Substantial subchondral bone restoration was observed. The tidemark was restored, with upwards migration of subchondral bone and an intralesional osteophyte. The worst results, with the poorest restoration of subchondral bone were observed in the AC and CFS groups, where marginal ossification surrounded central fibroses. Central cavities and subchondral cysts were present. Scarce scaffold remnants

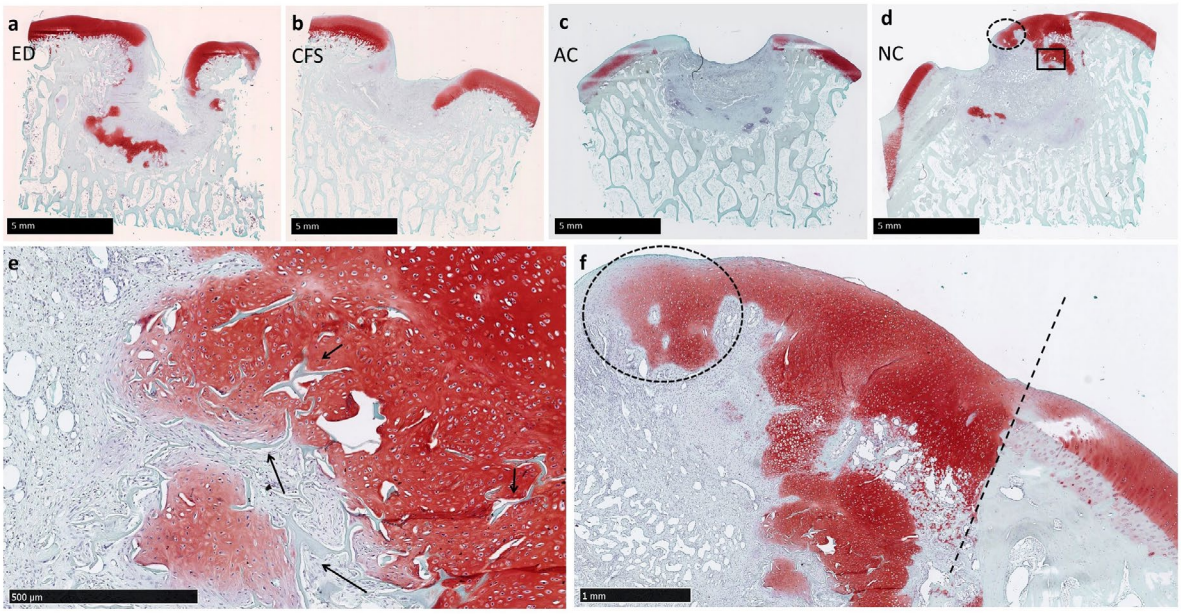

Fig. 5. Osteochondral sections of each group at 3 months stained with Safranin O (top row). (**a**) Details of the NC are pictured in the bottom row. Rectangle from NC is shown magnified. Hyaline cartilage stained red, with chondrocytes in lacunae and scaffold particles (arrows) embedded within cartilage. (**b**) On the right side of the bottom row an island of hyaline cartilage is encircled with dotted line. Straight dotted line marks the border between native cartilage on the right and implanted NC graft on the left.

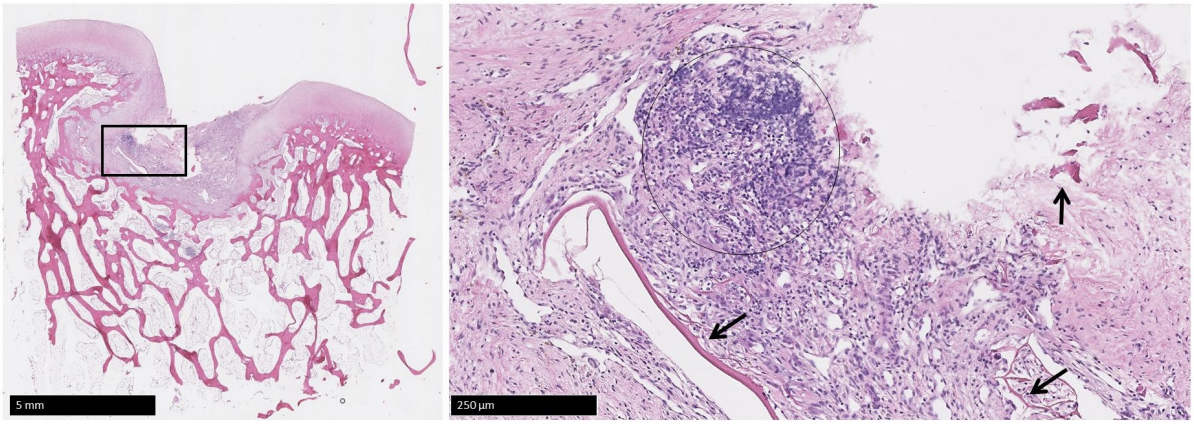

Fig. 6. The 6 weeks CFS sample from Fig. 4 is depicted again with the area in the rectangle magnified on the right side. Lymphocyte infiltration is shown in the circle. Arrows indicate the scaffold. HE staining.

were present in the AC and CFS group. The best osteochondral restoration was observed in the NC group. Articular cartilage and the subchondral bone displayed complete integration without demarcation. Restored cartilage was hyaline, with columnar chondrocyte organisation and an established tidemark. One sample had moderate subchondral plate migration (Fig. 11).

The overall ICRS II score was the highest for the NC group, but there was a significant difference only for one ICRS II parameter (Fig. 7**c**). Cell organisation scored significantly higher in NC compared to CFS group ($p = 0.046$). It was also significantly higher in AC compared to CFS ($p = 0.011$) and ED ($p = 0.02$) groups.

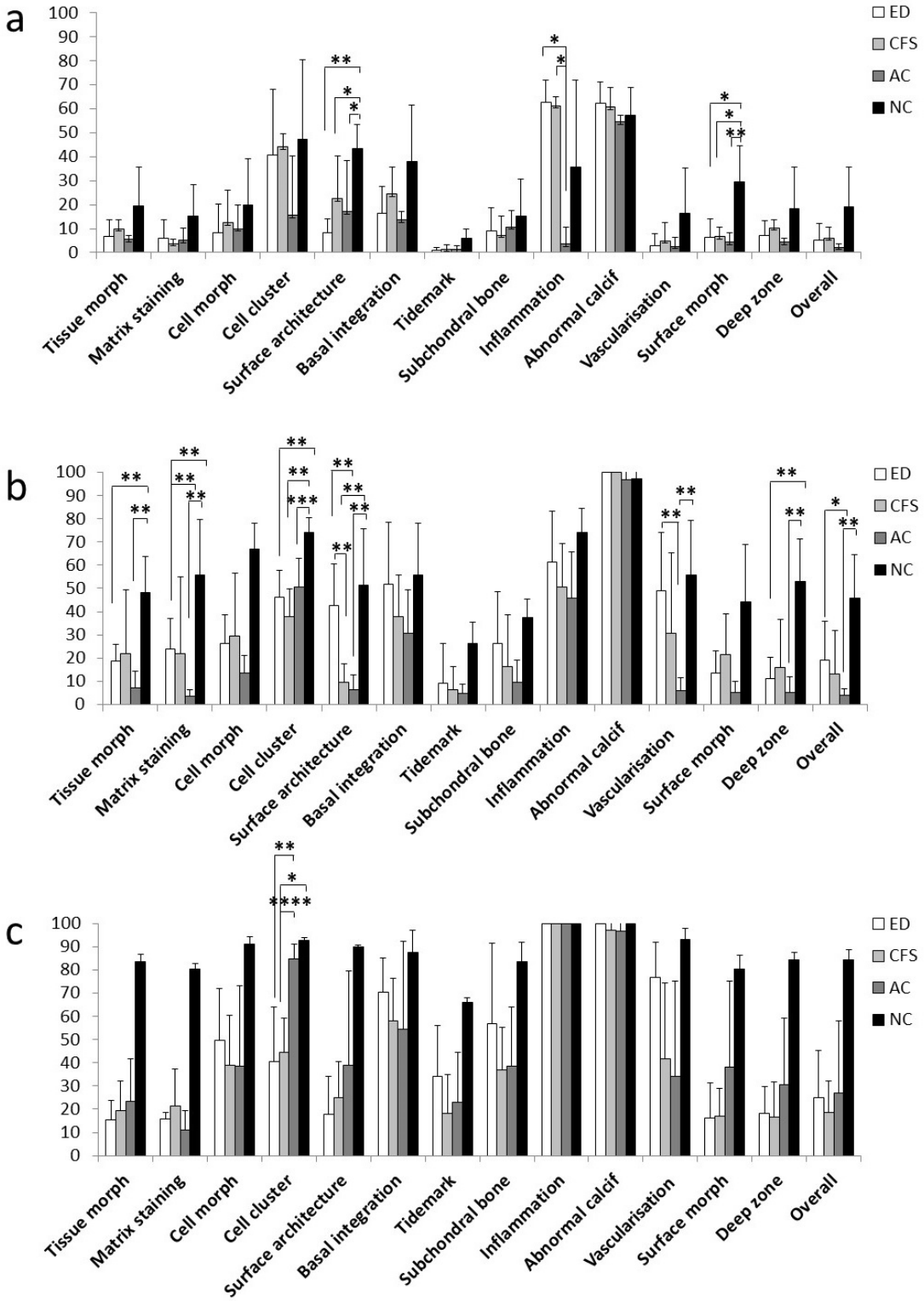

Fig. 7. ICRS II histology scores. (**a**) 6 weeks, (**b**) 3 months and (**c**) 12 months from chronic osteochondral defects treated with CFS, articular chondrocyte grafts (AC), nasal chondrocyte grafts (NC) or left without treatment (ED). Data are presented as mean ± SD. Statistically significant difference between connected columns is indicated with * $p = 0.043$, ** $p = 0.02$, *** $p = 0.028$ and **** $p = 0.011$.

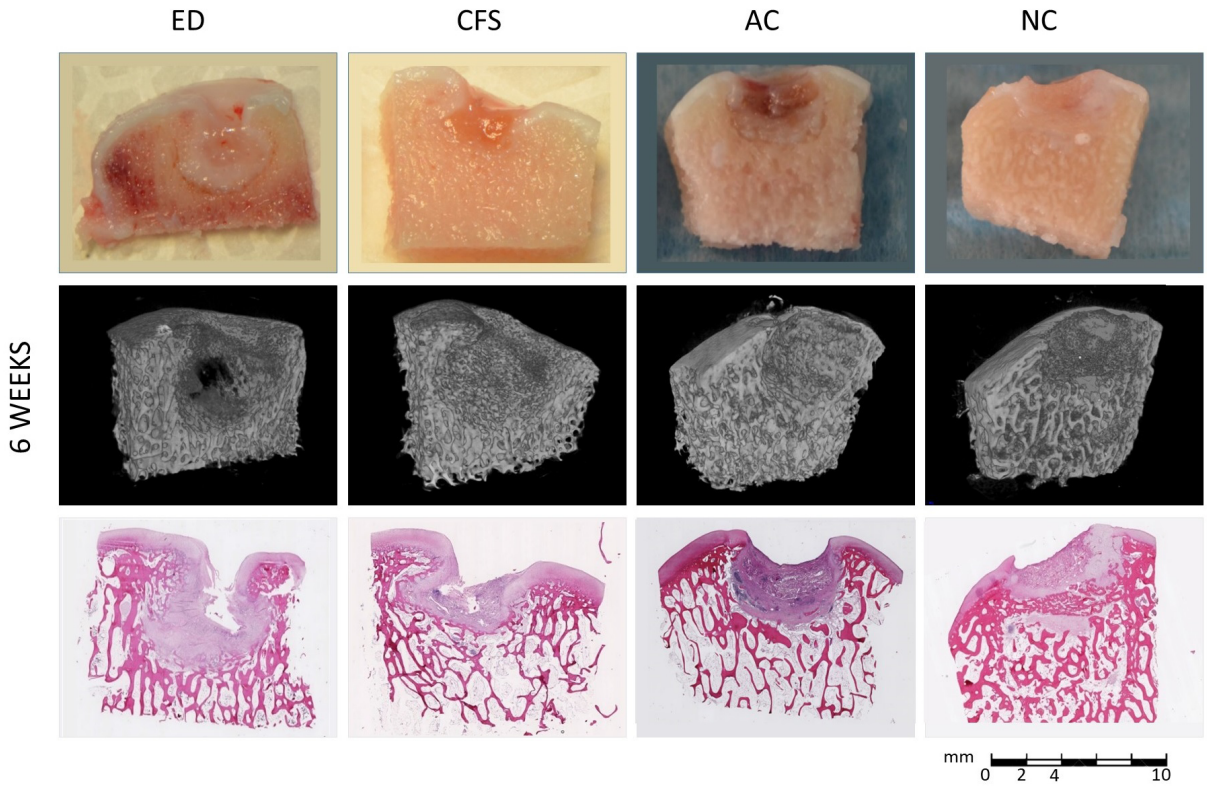

Fig. 8. Representative osteochondral blocks of each experimental group (*n* = 4 samples per group) in macroscopic view (top row), µCT 3D reconstructions (middle row) and sections stained with HE (bottom row) explanted 6 weeks after treatment.

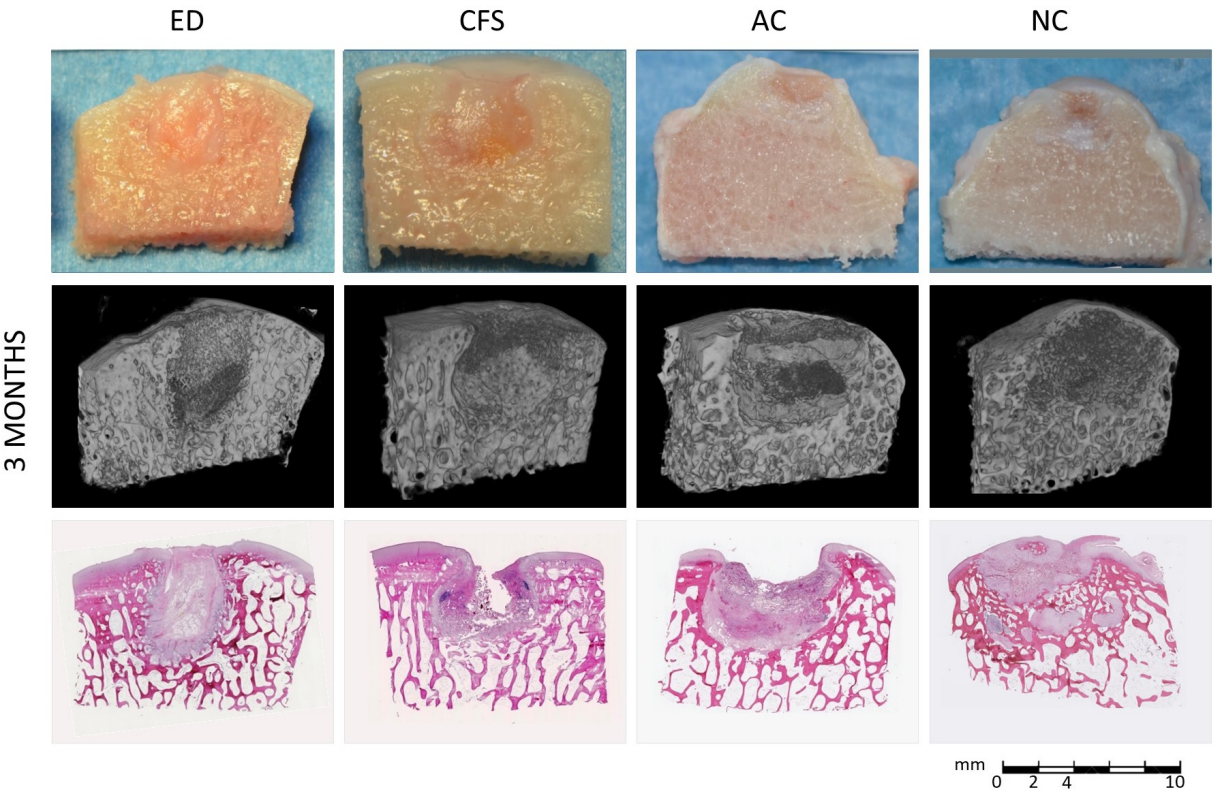

Fig. 9. Representative osteochondral blocks of each experimental group (*n* = 4 samples per group) in macroscopic view (top row), µCT 3D reconstructions (middle row) and sections stained with HE (bottom row) explanted 3 months after the treatment.

μCT analysis

μCT analysis at 6 weeks

At 6 weeks, μCT demonstrated the lack of mineralised tissue regeneration in all defects, with no appreciable plate or trabecular bone formation. Marginal subchondral ossification was sporadically observed. Some marginal trabecular resorption and remodelling with the loss of cylindrical shape was also noted (Fig. 7,8). For further μCT analysis, the defects were divided into regions: plate and trabecular bone. Quantifiable differences were found between all groups. Plate thickness was significantly higher in the AC, NC and ED compared to CFS (p = 0.021) group. Bone volume percent of the plate in the AC group was found to be higher compared to NC group (p = 0.034). AC plate was significantly less connected compared to CFS plate (p = 0.034). Trabecular bone was the thickest in the AC group and values were significantly higher than in CFS (p = 0.034) and NC (p = 0.034) groups. Detailed quantifiable differences among groups are shown in Fig. 12.

μCT analysis at 3 months

At 3 months, μCT images showed a lack of ossified tissue in the centre of all defects (presented with significant central cavities). However, bone formation was observed in plate and trabecular bone in all groups (Fig. 9). Trabecular bone volume increased compared to the previous time point. The formation of well-connected trabecular bone was present. Plate thickness after 3 months was more uniform across all groups. In the ED group, trabecular bone volume and surface area significantly increased, as compared to the AC group. Trabecular percent bone volume was significantly lower in AC compared to CFS (p = 0.043) and ED (p = 0.021) groups. ED plate had a significantly larger surface area than AC plate (p = 0.043). Bone surface area of AC trabecular bone was significantly smaller than ED (p = 0.043) and CFS trabecular bone (p = 0.021). AC group had significantly fewer trabeculae in trabecular bone compared to ED (p = 0.043) and CFS (p = 0.021) groups. Detailed quantifiable differences among groups are shown in Fig. 13.

μCT analysis at 12 months

At 12 months, the regeneration of trabecular bone was significant. However, there were still central cavities present, indicating non-osseous tissue. Overall, the best subchondral bone regeneration was found in the ED and NC groups. Trabecular structure was reconstituted with upward migration of the plate. Sclerotic changes were observed in the CFS group. AC group had the poorest trabecular bone regeneration. With the progression of subchondral bone healing, SMI values of the NC changed from positive at 3 months to negative at 12 months. SMI values of 0 and 3 represent the ideal plate and the ideal cylinder, but negative SMI values represent a 'negative space' (Issever *et al.*, 2003). As such, it is often seen in bone with many connections, forming 'saddles'. This trend could be a sign of a denser bone formation and was primarily seen in the NC group. Two NC samples had almost complete subchondral bone regeneration but due to low sample count did not reach statistical significance (Fig. 11). Detailed quantifiable differences among groups are shown in Fig. 14.

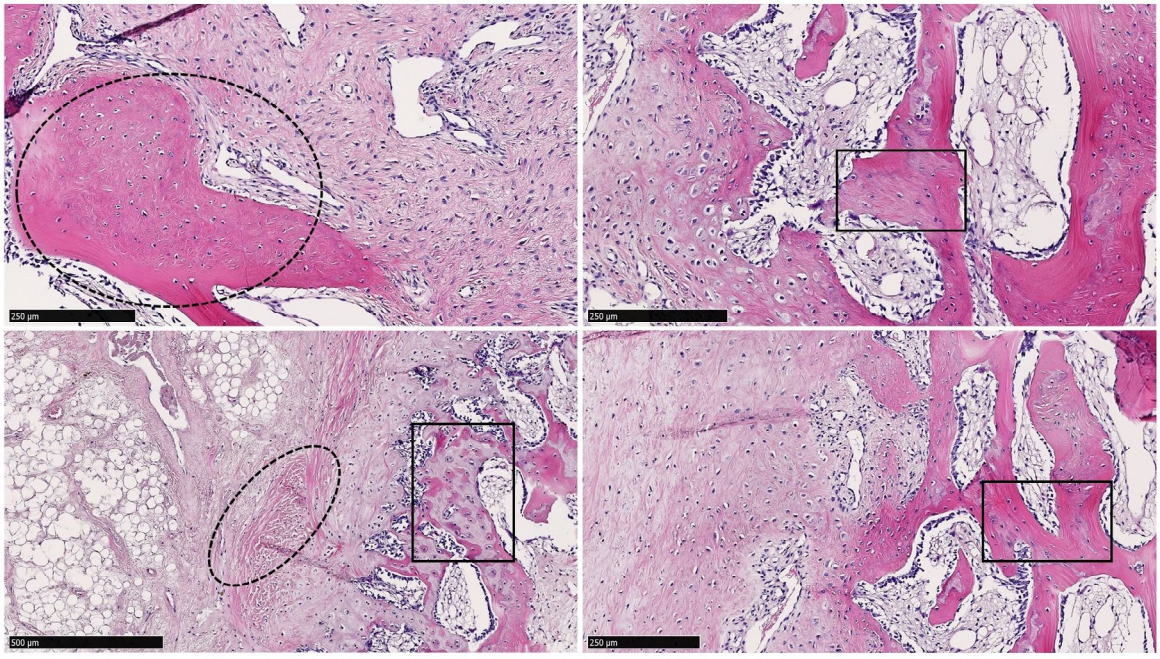

Fig. 10. ED at 3 months. Intramembranous (encircled with lined dots) and enchondral ossification (rectangles) were observed in the bottom of the defects. HE staining.

Discussion

The study was performed to address the challenge of using a clinically relevant large-animal model to test the feasibility of bioreactor-produced cartilage grafts for repair of osteochondral defects in humans. The aim was to produce a sizeable defect, which would correlate to a demanding clinical scenario. A previous study by Getgood *et al.* (2014) observed that empty osteochondral defects 5.8 mm in diameter, 6 mm deep heal moderately, with degenerative changes. Condyle size is a major determinant of possible defect sizes in animal models. Defects larger than 6 mm would produce a significant change in the curvature of the condyle and loss of joint surface contour. This could lead to significant changes in trans-articular force transfer, which could jeopardise defect site healing and the integrity of parent tissue (Bekkers *et al.*, 2013; Getgood *et al.*, 2012; Guettler *et al.*, 2004). It is the authors' opinion that the defect size of 6 mm (as done in the present study) was sufficient to achieve critical damage, in accordance with previous studies (Getgood *et al.*, 2012).

The press-fit fixation method was selected after performing a cadaver pilot study in which various fixation methods were tested, such as suturing a graft to articular cartilage and using a fibrin glue. A previous study (Filardo *et al.*, 2013) indicated that the use of fibrin glue does not contribute to additional mechanical stability but could interfere with the healing process and interpretation of the results. Transarticular sutures were also considered because they do add additional stability but at the high cost of inducing damage to the surrounding healthy cartilage. Therefore, the chosen method of rigid press-fit fixation was considered to be appropriate, reliable and recommendable.

Influence of the osteochondral graft transplantation procedure on subchondral bone microarchitecture and remodelling

The microarchitecture of the subchondral bone healing was compared following the autologous osteochondral implantation of bioreactor-produced AC and NC grafts, along with a CFS implant and spontaneous healing of an ED.

The results of histological and μCT analysis showed the best results in the NC group across all time points. Changes in the subchondral bone such as cyst appearance, bone resorption and impairment of the osseous microstructure were, to a lesser extent, present in all groups 6 weeks and 3 months after implantation. Marginal trabecular resorption and defect broadening was seen in all test groups, which resembled early OA changes, as observed in a recently described sheep translational model system (Oláh *et al.*, 2019). This happened early (6 weeks and 3 months) in the ED group, while later in the

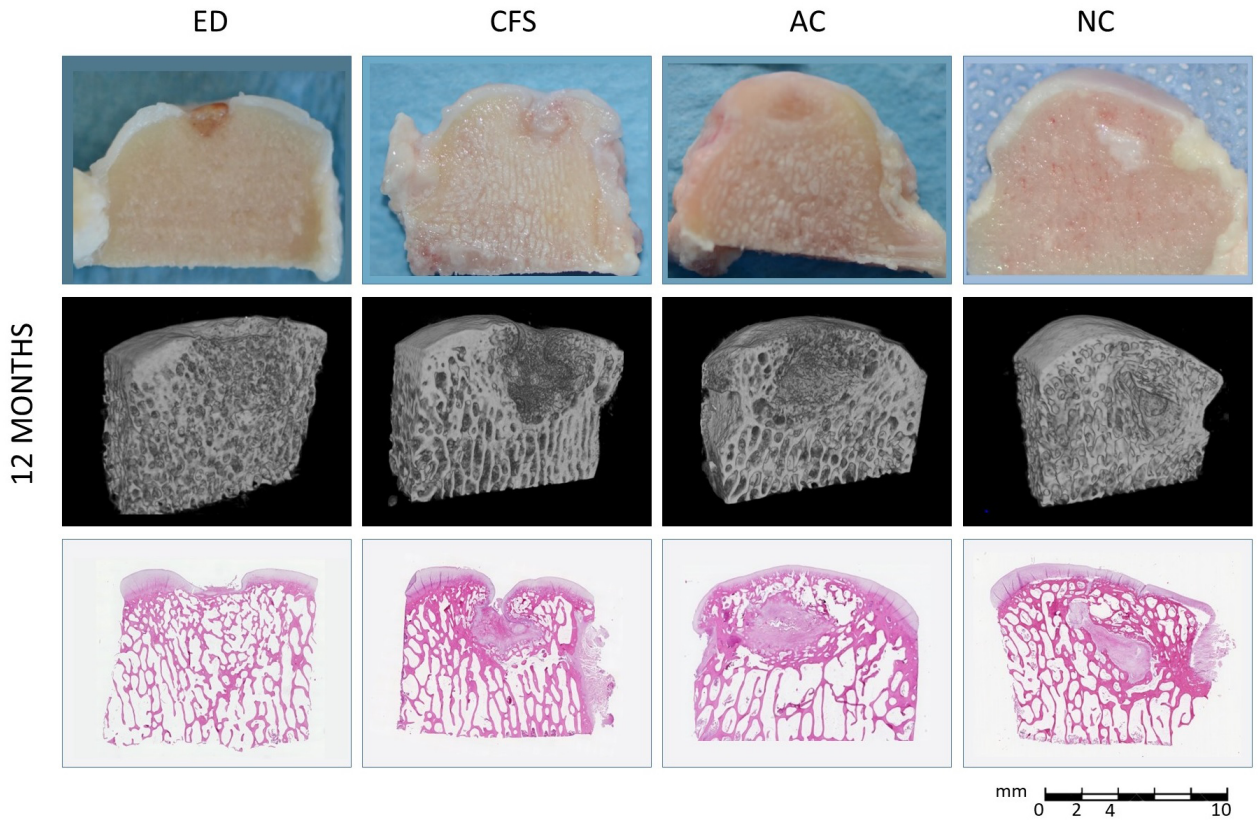

Fig. 11. Representative osteochondral blocks of each experimental group ($n = 4$ samples per group, except $n = 2$ for NC) in macroscopic view (top row), μCT 3D reconstructions (middle row) and sections stained with HE (bottom row). Explanted 12 months after treatment.

other groups (3 and 12 months). 12 months after implantation, an improvement in plate and trabecular bone repair was seen in all groups. As BV increased over time, and Conn.d decreased, it was concluded that the strength of the trabeculae increased, *i.e.* remodelling of the subchondral bone occurred (Ding *et al.*, 2003). This was also evident through the SMI value shift to negative in the NC group. A decrease in Tb.Sp and Conn.d over time indicated a decrease in porosity and formation of a stronger bone, which was observed in the NC group (Osterhoff *et al.*, 2016). Overall, it appeared that the presence of scaffold (both cell-free and seeded) inhibited trabecular development. Although the scaffold itself initially

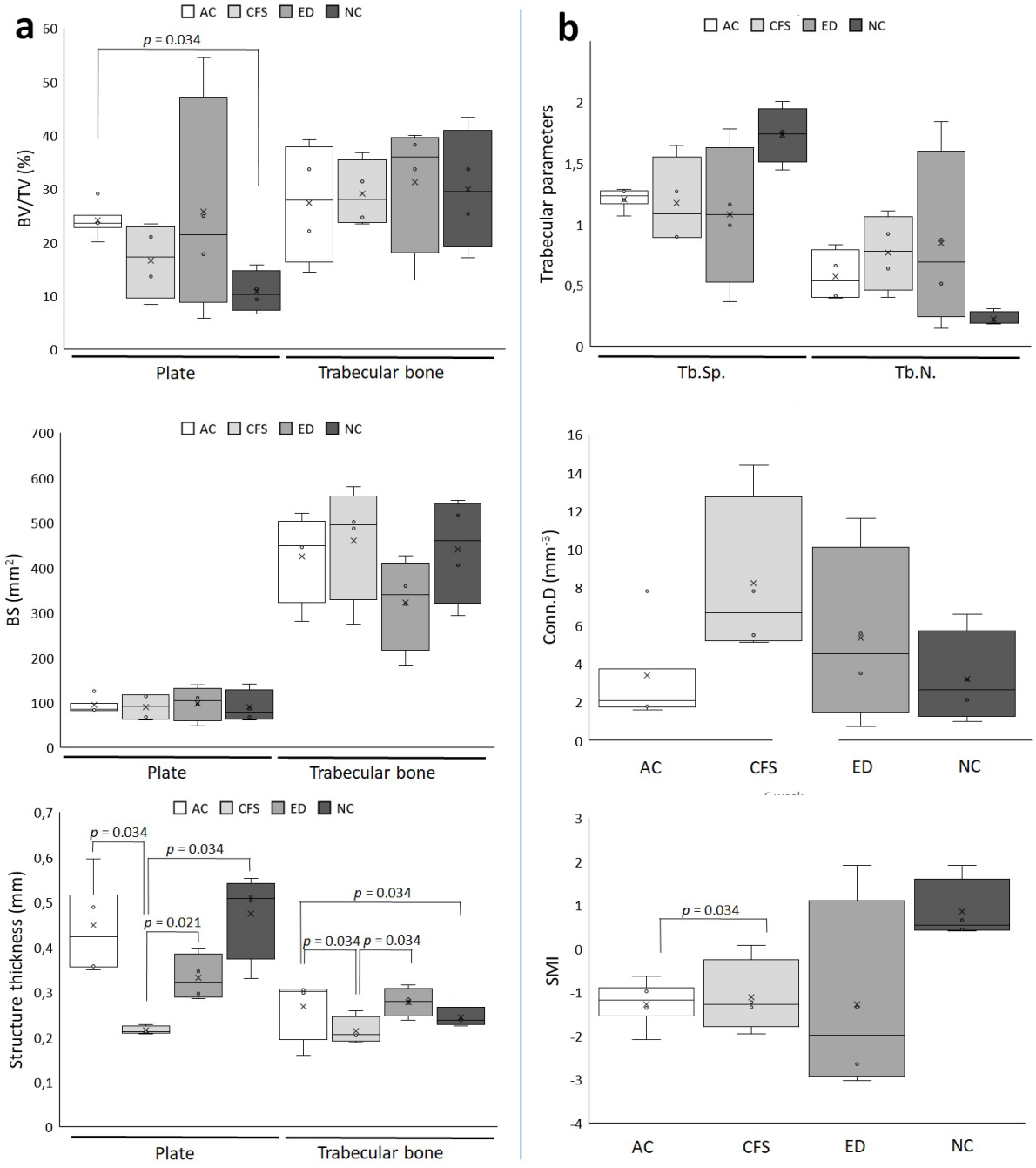

Fig. 12. Quantitative μCT analysis 6 weeks after treatment. (**a**) Common bone analysis revealed BV/TV, BS and cortical and trabecular thickness for the plate and trabecular bone, respectively. (**b**) Additional analysis of the trabecular bone showed Tb.Sp., Tb.N., Conn.D and SMI. Data are presented as median with data range, along with the mean. BV/TV value in the AC plate was significantly higher compared to NC plate ($p = 0.034$). Tb.Th value in the plate was significantly higher in AC ($p = 0.034$), NC ($p = 0.034$) and ED groups ($p = 0.021$) compared to CFS group. Conn.d value was significantly higher in CFS plate compared to AC plate ($p = 0.034$). Tb.Th value of the AC trabecular bone was significantly higher than CFS ($p = 0.034$) and NC ($p = 0.034$) trabecular bone. Tb.Th value of the ED trabecular bone was significantly higher compared to CFS trabecular bone ($p = 0.043$). Plate cortical thickness (equivalent to Tb.Th) in CFS was significantly lower than AC ($p = 0.034$), NC ($p = 0.034$) and ED ($p = 0.021$) groups.

provides mechanical reinforcement and attachment for cell and tissue ingrowth, in later phases its degradation triggers lytic response and may induce alterations to bone remodelling. A similar repair pattern was observed in a study by Sennett *et al.* (2021) in a Yucatan minipig model. More importantly, Christensen *et al.* (2016) reported this observation for humans.

Influence of different treatment groups on subchondral bone microarchitecture and remodelling

Healing of untreated osteochondral defects resembled the progression of OA (Orth *et al.*, 2013). Even though the present study used a small number of experimental animals, the best restoration of subchondral bone was observed when the defects

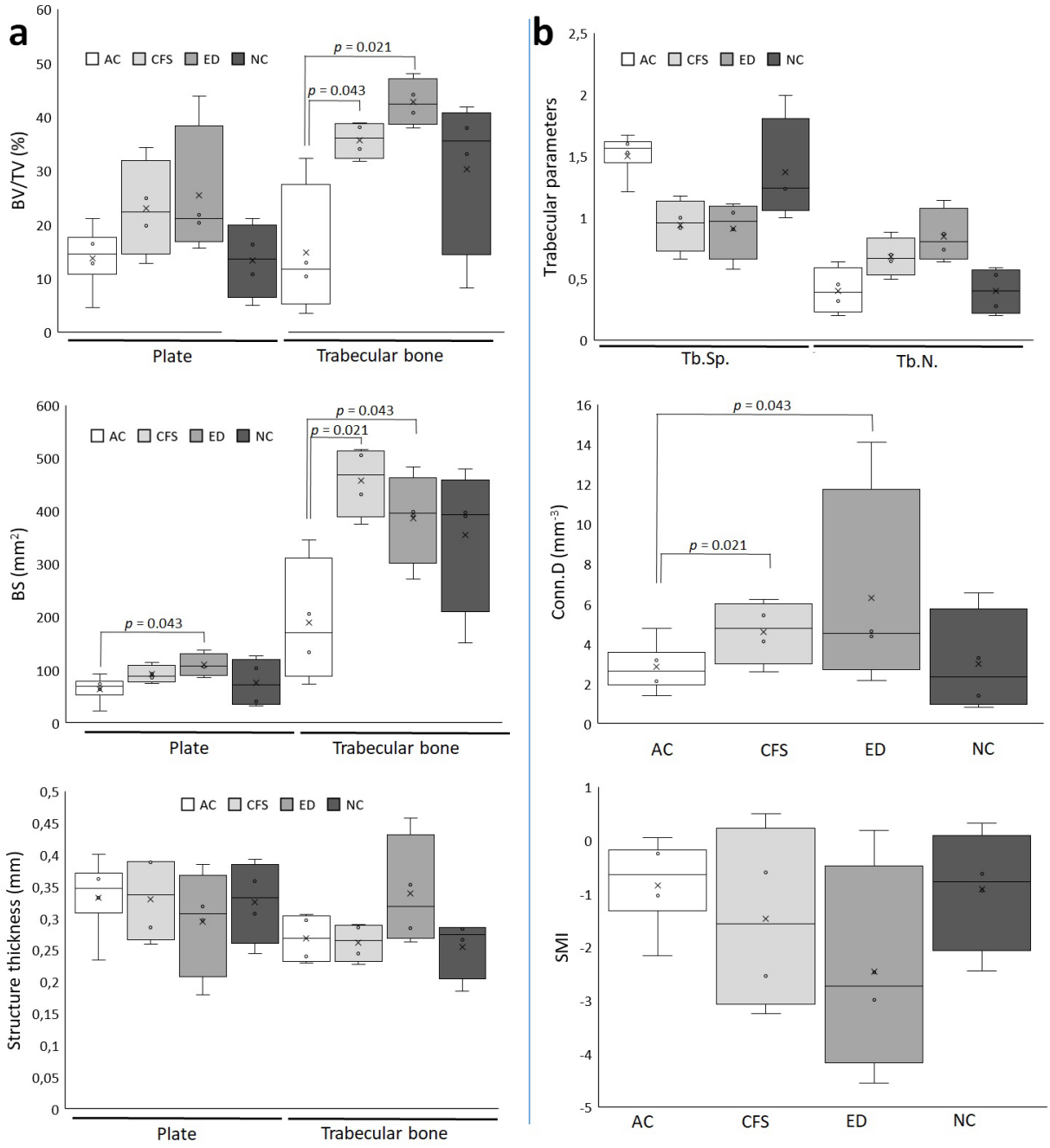

Fig. 13. µCT analysis 3 months after treatment. (**a**) Common bone analysis revealed BV/TV, BS and cortical and trabecular thickness for the plate and trabecular bone, respectively. (**b**) Additional analysis of the trabecular bone showed Tb.Sp., Tb.N., Conn.D and SMI. Data are presented as median with data range, along with the mean. Trabecular bone BV/TV value was significantly lower in AC compared to CFS (p = 0.043) and ED (p = 0.021) groups. BS value of ED plate was significantly higher than AC plate (p = 0.043). BS value of AC trabecular bone was significantly lower than ED (p = 0.043) and CFS trabecular bone (p = 0.021). Tb.N value was also significantly lower in AC trabecular bone compared to ED (p = 0.043) and CFS trabecular bone (p = 0.021).

were treated with NC grafts. Furthermore, OA alterations to the subchondral bone (upward migration of the subchondral plate, intralesional osteophytes, subchondral cysts and impairment of the osseous microstructure) were least expressed in the NC group at the final time point. This also suggested that nasal septum chondrocyte-seeded grafts adapted well to the biomechanical conditions of the loaded joint surface *in vivo* (Candrian *et al.*, 2008). Restoration of defects with AC grafts and CFS was not as good. A possible explanation could be that CFSs provided good repair in the short term but were not sufficient to restore larger defects in the long term (Christensen *et al.*, 2016). Also, poor repair observed with AC grafts could be explained by poor regenerative capacity of adult chondrocytes (Scotti *et al.*, 2012; Tay *et al.*, 2004). The CFS and ED defects were similarly reluctant to heal at early time points, being engaged in connective tissue formation. A similar phenomenon was observed by Sennett *et al.* (2021), who suggested that CFS placement results in reduced healing caused by a subchondral bone remodelling response. This tissue response was particularly visible at 3 months. Perhaps surprisingly, at the end of the

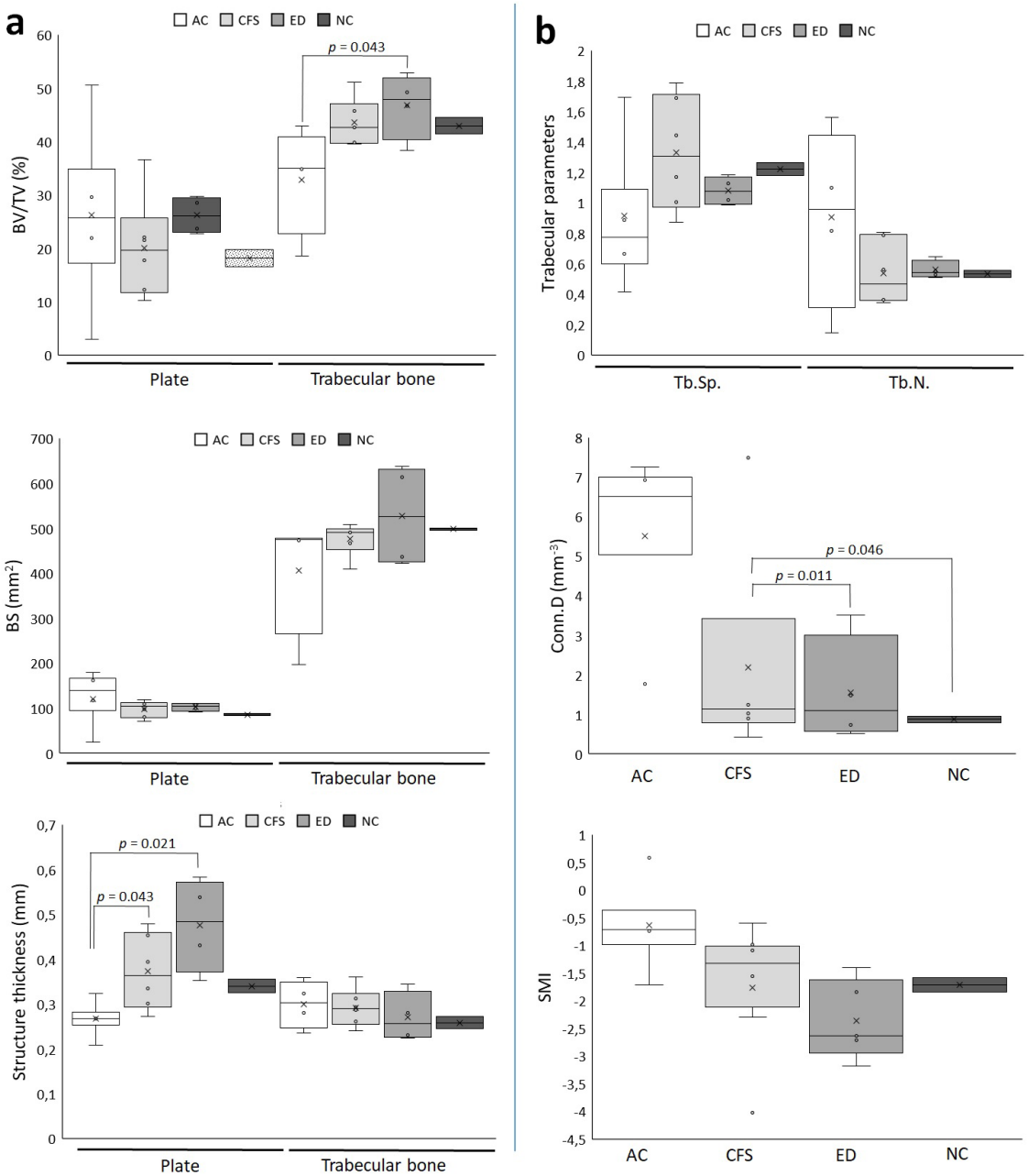

Fig. 14. Quantitative μCT analysis 12 months after treatment. (**a**) Common bone analysis revealed BV/TV, BS and cortical and trabecular thickness for the plate and trabecular bone, respectively. (**b**) Additional analysis of the trabecular bone showed Tb.Sp., Tb.N., Conn.D and SMI. Data are presented as median with data range, along with the mean. Trabecular bone BV/TV value was significantly lower in AC compared to ED ($p = 0.043$) group. Plate cortical thickness (equivalent to Tb.Th) value in AC was significantly lower than CFS ($p = 0.034$) and ED ($p = 0.021$) groups. Trabecular bone Conn.d value in CFS was significantly higher than ED ($p = 0.011$) and NC ($p = 0.046$) groups.

study, both groups showed a trend towards improved repair in trabecular and subchondral plate restoration compared to the AC group. By the end of the study, ED group specimens displayed a more remodelled, highly trabecular structure. Delayed restoring of the trabecular structure could be due to the presence of the scaffold in other groups. The NC group had observable restoration of the osteochondral unit, with fewest alterations to the subchondral bone associated with OA.

The treatment of knee chondral and osteochondral lesions poses a great challenge for orthopaedic surgeons. The development of innovative scaffolds to be used in these demanding clinical scenarios brought both new hope and new challenges. Implantation of biomimetic scaffolds with or without cells at the lesion site promotes tissue repair, with physiological and mechanical properties that are similar to the native tissue. On the other hand, the presence of the scaffold and its subsequent degradation may induce an inflammatory response that can interfere with bone remodelling and cartilage formation. A biomimetic approach has been adopted in the development of the bi-phasic scaffold used in the present study. The upper layer was made of collagen to target cartilage regeneration and the bottom layer of bioactive Mg-HA, which was co-precipitated with collagen and targeted subchondral bone integration (Fig. 15). Although many different clinical studies have shown promising results at mid-term follow-up, there are some concerns about the true potential of this technology (Christensen *et al.*, 2016; D'Ambrosi *et al.*, 2019). In addition, clinical studies do not offer the possibility of analysing in detail the microarchitecture and morphology of the tissues involved. Hence, it is of utmost importance to collect the data from the translational animal models.

Large-animal studies on sheep, goats and pigs (Dias *et al.*, 2018; Lane *et al.*, 2004; Madry *et al.*, 2015) have been instrumental in OA and cartilage repair research, since many strong similarities exist between the human and ovine knee joints (Madry *et al.*, 2015; Osterhoff *et al.*, 2011). The characterisation of subchondral bone repair in sheep models possibly provides a glimpse into subchondral bone repair in human patients and can help determine the quality of long-term osteochondral defect treatment. Hence, the selection of sheep for a study of this scope and duration was appropriate. Moreover, the methodology and technology used can not only be translated to other large-animal models but also to humans, giving translational value to the study (Dias *et al.*, 2018; Sennett *et al.*, 2021). The present study provided admissible evidence for a viable nasal septum chondrocyte-based graft treatment of critical osteochondral articular defects in sheep and, as such, provided translational value. This was evidenced by the extent of new-tissue formation and the best integration of new tissue into the surrounding tissue in the NC group throughout all time points in the study.

Limitations

The weight and age of the sheep varied and it is possible that this attributed to the heterogeneity of the samples. For the nature of the study, it would have been desirable for the test animals to be approximately of the same age, with a permissible difference of only a few months.

Further drawbacks of the study were the small number of animals, large number of test groups and many time points to which the total number of specimens was distributed. 3 time points were selected due to the commitment to monitor the trend

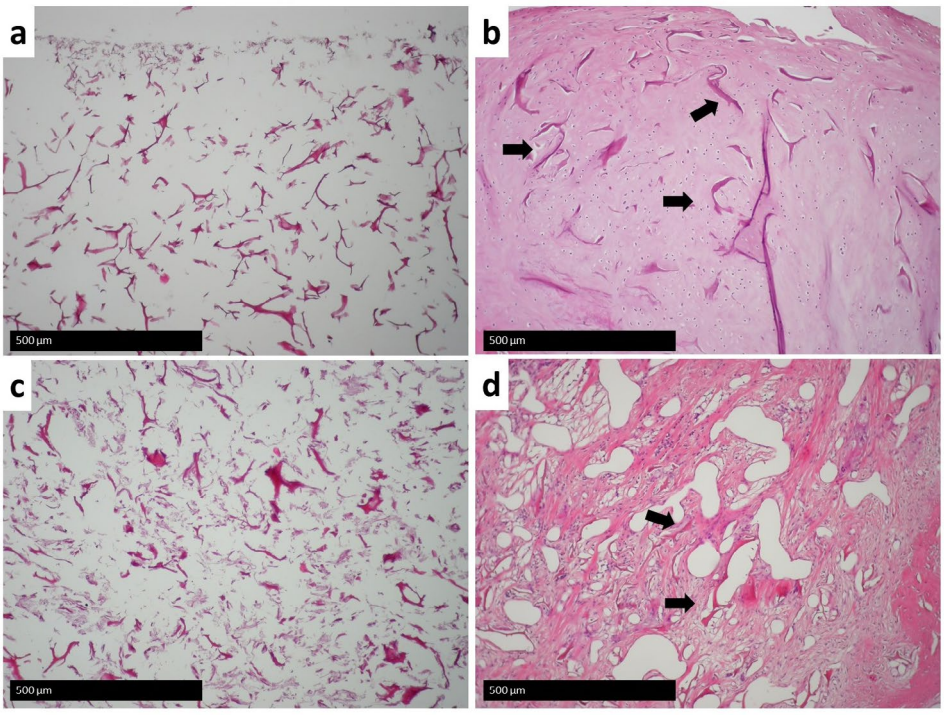

Fig. 15. Histology of the unseeded, non-cultivated scaffold. (**a**) Cartilage layer of the scaffold, (**b**) bony layer of the scaffold, (**c**) NC implanted defect and (**d**) CFS implanted defect at 3 months. Arrows indicate scaffold particles. HE staining.

and the healing process of the osteochondral unit. The attempt was made to minimise this deficit by using both femoral condyles (medial and lateral), thus doubling the number of samples without increasing the number of animals. The disadvantage of such approach is the inevitable comparison of medial and lateral condyles as equivalent specimens, even though there is a difference in the microarchitecture of the subchondral bone between the weight-bearing (medial) and non-weight-bearing (lateral) condyles. Namely, regional differences in the density of the subchondral plate are observed in the regions of the joints under different loads (Madry *et al.*, 2010). Heterogeneity in the structure of the subchondral bone of unoperated condyles was also observed in the present study. This phenomenon illustrates the importance of defect site choice, as well as the pitfall of presumption of microarchitecture homogeneity across the joint.

The subchondral plate is defined as top 1.4 mm of the ROI (Hirvasniemi *et al*., 2016). This does not necessarily coincide with the actual subchondral plate, especially at early time points of evaluation. Although signs of defect mineralisation are also encountered at early time points, due to the limited amount of mineral tissue, μCT analysis has its constraints. At early time points, histological and immunohistochemical methods are much more suitable for tissue analysis. Apart from insight into tissue structure, they also show the activity of individual cell types.

For practical and financial reasons, most large-animal studies last from 2 weeks to 18 months (Dias *et al.*, 2018). The physiological reaction to marrow stimulation procedures is described as early bone resorption followed by a remodelling process resembling fracture healing (Heir *et al.*, 2012). The duration of this remodelling phase depends on the experimental model and ranges between 3 and 12 months (Dorotka *et al.*, 2005; Lane *et al.*, 2004; Nam *et al.*, 2004). The present study was completed 12 months after graft implantation and bone remodelling in scaffold groups was still ongoing. A longer period, from 12 to 24 months, is required for complete healing or maturation of the tissue (Dias *et al.*, 2018; Hoemann *et al.*, 2011; Pilichi *et al.*, 2014). The fact remains that bone remodelling is a long-lasting, dynamic process and that the samples in the present study did not show complete filling of bone defects.

Conclusions

Structural remodelling of the subchondral bone is an important part of the osteochondral repair process. The present study confirmed that a longer follow-up was needed to acquire data relevant for clinical translation. Apart from the 12 month time point, two earlier time points were added to get better insight into the early changes that occurred following graft transplantation as well as to evaluate stability of the graft implanted. Results showed that press-fit fixation was appropriate, reliable and recommendable. Furthermore, the study also showed that the presented strategy (involving tissue engineering of bioreactor-based osteochondral grafts) was safe and feasible, the chosen large-animal model and study duration appropriate and the methodology and technology used translatable not only to other large-animal models but also to humans. Finally, it is of utmost importance to expand on the insight gathered in the present study and further studies with larger experimental groups are necessary to elucidate the observed phenomena.

Acknowledgements

This project received fundings from the European Union's Seventh Program for research, technological development and demonstration under Grant Agreement No. 278807 (BIO-COMET).

References

Calabrese G, Giuffrida R, Fabbi C, Figallo E, Lo Furno D, Gulino R, Colarossi C, Fullone F, Giuffrida R, Parenti R, Memeo L, Forte S (2016) Collagen-hydroxyapatite scaffolds induce human adipose derived stem cells osteogenic differentiation *in vitro*. PLoS One **11**: e0151181. DOI: 10.1371/journal.pone.0151181.

Candrian C, Vonwil D, Barbero A, Bonacina E, Miot S, Farhadi J, Wirz D, Dickinson S, Hollander A, Jakob M, Li Z, Alini M, Heberer M, Martin I (2008) Engineered cartilage generated by nasal chondrocytes is responsive to physical forces resembling joint loading. Arthritis Rheum **58**: 197-208.

Christensen BB, Foldager CB, Jensen J, Jensen NC, Lind M (2016) Poor osteochondral repair by a biomimetic collagen scaffold: 1- to 3-year clinical and radiological follow-up. Knee Surg Sports Traumatol Arthrosc **24**: 2380-2387.

D'Ambrosi R, Valli F, De Luca P, Ursino N, Usuelli FG (2019) MaioRegen osteochondral substitute for the treatment of knee defects: a systematic review of the literature. J Clin Med. **8**: 783-797.

Dempster DW, Compston JE, Drezner MK, Glorieux FH, Kanis JA, Malluche H, Meunier PJ, Ott SM, Recker RR, Parfitt AM (2013) Standardized nomenclature, symbols, and units for bone histomorphometry: a 2012 update of the report of the ASBMR Histomorphometry Nomenclature Committee. J Bone Miner Res **28**: 2-17.

Dias IR, Viegas PA, Carvalho PP (2018) Large animal models for osteochondral regeneration. Adv Exp Med Biol **1059**: 441-501.

Ding M, Odgaard A, Hvid I (2003) Changes in the three-dimensional microstructure of human tibial cancellous bone in early osteoarthritis. J Bone Joint Surg Br **85**: 906-912.

Dorotka R, Bindreiter U, Macfelda K, Windberger U, Nehrer S (2005) Marrow stimulation and chondrocyte transplantation using a collagen matrix for cartilage repair. Osteoarthritis Cartilage **13**: 655-664.

Duncan H, Jundt J, Riddle JM, Pitchford W, Christopherson T (1987) The tibial subchondral plate. A scanning electron microscopic study. J Bone Joint Surg Am **69**: 1212-1220.

Feldkamp LA, Goldstein SA, Parfitt AM, Jesion G, Kleerekoper M (1989) The direct examination of three-dimensional bone architecture *in vitro* by computed tomography. J Bone Miner Res **4**: 3-11.

Filardo G, Kon E, Perdisa F, Di Matteo B, Di Martino A, Iacono F, Zaffagnini S, Balboni F, Vaccari V, Marcacci M (2013) Osteochondral scaffold reconstruction for complex knee lesions: a comparative evaluation. Knee **20**: 570-576.

Fisher MB, Belkin NS, Milby AH, Henning EA, Bostrom M, Kim M, Pfeifer C, Meloni G, Dodge GR, Burdick JA, Schaer TP, Steinberg DR, Mauck RL (2015) Cartilage repair and subchondral bone remodeling in response to focal lesions in a mini-pig model: implications for tissue engineering. Tissue Eng Part A **3-4**: 850-860.

Getgood A, Henson F, Skelton C, Brooks R, Guehring H, Fortier LA, Rushton N (2014) Osteochondral tissue engineering using a biphasic collagen/GAG scaffold containing rhFGF18 or BMP-7 in an ovine model. J Exp Orthop **1**: 13. DOI: 10.1186/s40634-014-0013-x.

Goldring SR, Soldring MB (2016) Changes in the osteochondral unit during osteoarthritis: structure, function and cartilage-bone crosstalk. Nat Rev Rheumatol **12**: 632-664.

Gomoll AH, Madry H, Knutsen G, van Dijk N, Seil R, Brittberg M, Kon E (2010) The sub-chondral bone in articular cartilage repair: current problems in the surgical management. Knee Surg Sports Traumatol Arthrosc **18**: 434-447.

Hildebrand T, Rüegsegger P (1997) Quantification of bone microarchitecture with the structure model index. Comput Methods Biomech Biomed Engin **1**: 15-23.

Hirvasniemi J, Thevenot J, Kokkonen HT, Finnilä MA, Venäläinen MS, Jämsä T, Korhonen RK, Töyräs J, Saarakkala S (2016) Correlation of subchondral bone density and structure from plain radiographs with micro computed tomography *ex vivo*. Ann Biomed Eng **44**: 1698-1709.

Hoemann C, Kandel R, Roberts S, Saris DB, Creemers L, Mainil-Varlet P, Méthot S, Hollander AP, Buschmann MD (2011) International Cartilage Repair Society (ICRS) recommended guidelines for histological endpoints for cartilage repair studies in animal models and clinical trials. Cartilage **2**: 153-172.

Issever AS, Burghardt A, Patel V, Laib A, Lu Y, Ries M, Majumdar S (2003) A micro-computed tomography study of the trabecular bone structure in the femoral head. J Musculoskelet Neuronal Interact **3**: 176-184.

Jeon JE, Vaquette C, Klein TJ, Hutmacher DW (2014) Perspectives in multiphasic osteochondral tissue engineering. Anat Rec (Hoboken) **297**: 26-35.

Kon E, Delcogliano M, Filardo G, Fini M, Giavaresi G, Francioli S, Martin I, Pressato D, Arcangeli E, Quarto R, Sandri M, Marcacci M (2010) Orderly osteochondral regeneration in a sheep model using a novel nano-composite multilayered biomaterial. J Orthop Res **28**: 116-124.

Lajeunesse D, Hilal G, Pelletier JP, Martel-Pelletier J (1999) Subchondral bone morphological and biochemical alterations in osteoarthritis. Osteoarthritis Cartilage **7**: 321-322.

Lane JG, Massie JB, Ball ST, Amiel ME, Chen AC, Bae WC, Sah RL, Amiel D (2004) Follow-up of osteochondral plug transfers in a goat model: a 6-month study. Am J Sports Med **32**: 1440-1450.

Lee JK, Responte DJ, Cissell DD, Hu JC, Nolta JA, Athanasiou KA (2014) Clinical translation of stem cells: insight for cartilage therapies. Crit Rev Biotechnol **34**: 89-100.

Lepage SIM, Robson N, Gilmore H, Davis O, Hooper A, St John S, Kamesan V, Gelis P, Carvajal D, Hurtig M, Koch TG (2019) Beyond cartilage repair: the role of the osteochondral unit in joint health and disease. Tissue Eng Part B Rev **25**: 114-125.

Madry H, van Dijk CN, Mueller-Gerbl M 2010) The basic science of the subchondral bone. Knee Surg Sports Traumatol Arthrosc **18**: 419-433.

Madry H, Ochi M, Cucchiarini M, Pape D, Seil R (2015) Large animal models in experimental knee sports surgery focus on clinical translation. J Exp Ortop **2**: 9. DOI: 10.1186/s40634-015-0025-1.

Mainil-Varlet P, Van Damme B, Nesic D, Knutsen G, Kandel R, Roberts S (2010) A new histology scoring system for the assessment of the quality of human cartilage repair: ICRS II. Am J Sports Med **38(5)**: 880-890.

Malda J, van Blitterswijk CA, van Geffen M, Martens DE, Tramper J, Riesle J (2014) Low oxygen tension stimulates the redifferentiation of dedifferentiated adult human nasal chondrocytes. Osteoarthritis Cartilage **12**: 306-313.

Manferdini C, Cavallo C, Grigolo B, Fiorini M, Nicoletti A, Gabusi E, Zini N, Pressato D, Facchini A, Lisignoli G (2016) Specific inductive potential of a novel nanocomposite biomimetic biomaterial for osteochondral tissue regeneration. J Tissue Eng Regen Med **10**: 374-391.

Milz S, Putz R (1994) Quantitative morphology of the subchondral plate of the tibial plateau. J Anat **185**: 103-110.

Mithoefer K, Williams RJ, 3rd, Warren RF, Potter HG, Spock CR, Jones EC, Wickiewicz TL, Marx RG (2005) The microfracture technique for the treatment of articular cartilage lesions in the knee. A prospective cohort study. J Bone Joint Surg Am **87**: 1911-1920.

Mumme M, Steinitz A, Nuss KM, Klein K, Feliciano S, Kronen P, Jakob M, von Rechenberg B, Martin I, Barbero A, Pelttari K (2016a) Regenerative potential of tissue-engineered nasal chondrocytes in

goat articular cartilage defects. Tissue Eng Part A **22**: 1286-1295.

Mumme M, Barbero A, Miot S, Wixmerten A, Feliciano S, Wolf F, Asnaghi AM, Baumhoer D, Bieri O, Kretzschmar M, Pagenstert G, Haug M, Schaefer DJ, Martin I, Jakob M (2016b) Nasal chondrocyte-based engineered autologous cartilage tissue for repair of articular cartilage defects: an observational first-in-human trial. Lancet **388**: 1985-1994.

Nafei A, Danielsen CC, Linde F, Hvid I (2000) Properties of growing trabecular ovine bone. Part I: mechanical and physical properties. J Bone Joint Surg Br **82**: 910-920.

Nikolaou VS, Giannoudis PV (2017) History of osteochondral allograft transplantation. Injury **48**: 1283-1286.

Oláh T, Reinhard J, Gao L, Haberkamp S, Goebel LKH, Cucchiarini M, Madry H (2019) Topographic modeling of early human osteoarthritis in sheep. Sci Transl Med **11**: eaax6775. DOI: 10.1126/scitranslmed.aax6775.

Orth P, Cucchiarini M, Kohn D, Madry H (2011) Alterations of the subchondral bone in osteochondral repair–translational data and clinical evidence. Eur Cell Mater **28**: 299-316.

Osterhoff G, Löffler S, Steinke H, Feja C, Josten C, Hepp P (2011) Comparative anatomical measurements of osseous structures in the ovine and human knee. Knee **18**: 98-103.

Osterhoff G, Morgan EF, Shefelbine SJ, Karim L, McNamara LM, Augat P (2016) Bone mechanical properties and changes with osteoporosis. Injury **47**: 11-20.

Pape D, Filardo G, Kon E, van Dijk CN, Madry H (2010) Disease-specific clinical problems associated with the subchondral bone. Knee Surg Sports Traumatol Arthrosc **18**: 448-462.

Pilichi S, Rocca S, Dattena M, Pool RR, Mara L, Sanna D, Masala G, Manunta ML, Dore S, Manunta A, Passino ES (2018) Sheep embryonic stem-like cells engrafted into sheep femoral condyle osteochondral defects: 4-year follow-up. BMC Vet Res **28**: 213. DOI: 10.1186/s12917-018-1532-y.

Salmon PL (2020) Micro-computed tomography (μCT) in medicine and engineering. Editor: Orhan K. Springer Nature Switzerland. pp: 49-75.

Saris DB, Vanlauwe J, Victor J, Almqvist KF, Verdonk R, Bellemans J, Luyten FP (2009) Treatment of symptomatic cartilage defects of the knee: characterized chondrocyte implantation results in better clinical outcome at 36 months in a randomized trial compared to microfracture. Am J Sports Med **37 Suppl 1**: 10S-19S.

Sajjadian A, Rubinstein R, Naghshineh N (2010) Current status of grafts and implants in rhinoplasty: part I. Autologous grafts. Plast Reconstr Surg **125**: 40e-49e.

Scotti C, Osmokrovic A, Wolf F, Miot S, Peretti GM, Barbero A, Martin I (2012) Response of human engineered cartilage based on articular or nasal chondrocytes to interleukin-1beta and low oxygen. Tissue Eng Part A **18**: 362-372.

Sennett ML, Friedman JM, Ashley BS, Stoeckl BD, Patel JM, Alini M, Cucchiarini M, Eglin D, Madry H, Mata A, Semino C, Stoddart MJ, Johnstone B, Moutos FT, Estes BT, Guilak F, Mauck RL, Dodge GR (2021) Long term outcomes of biomaterial-mediated repair of focal cartilage defects in a large animal model. Eur Cell Mater **41**: 40-51.

Siu WS, Qin L, Cheung WH, Leung KS (2004) A study of trabecular bones in ovariectomized goats with micro-computed tomography and peripheral quantitative computed tomography Bone **35**: 21-26.

Tampieri A, Sandri M, Landi E, Pressato D, Francioli S, Quarto R, Martin I (2008) Design of graded biomimetic osteochondral composite scaffolds. Biomaterials **29**: 3539-3546.

Tay AG, Farhadi J, Suetterlin R, Pierer G, Heberer M, Martin I (2004) Cell yield, proliferation, and postexpansion differentiation capacity of human ear, nasal, and rib chondrocytes. Tissue Eng **10**: 762-770.

Tonnarelli B, Santoro R, Asnaghi MA, Wendt D (2016) Streamlined bioreactor-based production of human cartilage tissues. Eur Cell Mater **31**: 382-394.

Vukasovic A, Asnaghi MA, Kostesic P, Quasnichka H, Cozzolino C, Pusic M, Hails L, Trainor N, Krause C, Figallo E, Filardo G, Kon E, Wixmerten A, Maticic D, Pellegrini G, Kafienah W, Hudetz D, Smith T, Martin I, Ivkovic A, Wendt D (2019) Bioreactor-manufactured cartilage grafts repair acute and chronic osteochondral defects in large animal studies. Cell Prolif **52**: e12653. DOI: 10.1111/cpr.12653.

Wendt D, Jakob M, Martin I (2005) Bioreactor-based engineering of osteochondral grafts: from model systems to tissue manufacturing. J Biosci Bioeng **100**: 489-494.

Discussion with Reviewer

Reviewer: Could an osteochondral scaffold generated with AC display a less mature cartilaginous extracellular matrix, with decreased glycosaminoglycan and/or type II collagen content and, thus, inferior biomechanical features?
Authors: According to Lehoczky *et al.* (2020, additional reference), the cartilage-forming capacity of debrided knee chondrocytes is reduced when compared to nasal septum chondrocytes. In their study, the glycosaminoglycan levels in debrided knee chondrocytes-engineered grafts were relatively low and type II collagen virtually absent, thus producing a tissue with limited or undetectable matrix components.

Reviewer: Could such biomechanic differences in the implanted scaffolds contribute to the observed superior performance of NCs, in addition to the poor regenerative capacity of adult chondrocytes?

Authors: The biomechanical differences of different constructs before implantation were not tested. However, based on the evidence provided by others (Candrian *et al.*, 2007, additional reference), it could be the case. Candrian *et al.* (2007, additional reference) found that engineered cartilage generated by NCs (ECN) constructs showed a more intense and uniform staining for glycosaminoglycan and type II collagen than engineered cartilage generated by AC tissues. Consistently, the biochemically quantified amounts of glycosaminoglycan and type II collagen were significantly larger (71 % and 73 %, respectively) for ECN compared with ECA tissues. Further, engineered cartilage generated by AC constructs were overall less responsive to all mechanical loading regimens, likely due to the lower extracellular matrix content.

Reviewer: What is the rationale for comparing bioreactor-generated scaffolds with AC and NC constructs?

Authors: The rationale for comparing CFSs with bioreactor-manufactured AC and NC constructs was to see how an unseeded scaffold behaved in terms of tissue-healing potential, tissue integration and residue.

Additional References

Candrian C, Vonwil D, Barbero A, Bonacina E, Miot S, Farhadi J, Wirz D, Dickinson S, Hollander A, Jakob M, Li Z, Alini M, Heberer M, Martin I (2008) Engineered cartilage generated by nasal chondrocytes is responsive to physical forces resembling joint loading. Arthritis Rheum **58**: 197-208.

Lehoczky G, Wolf F, Mumme M, Gehmert S, Miot S, Haug M, Jakob M, Martin I, Barbero A (2020) Intra-individual comparison of human nasal chondrocytes and debrided knee chondrocytes: relevance for engineering autologous cartilage grafts. Clin Hemorheol Microcirc **74**: 67-78.

Editor's note: The Scientific Editor responsible for this paper was Chris Evans.